Journal of Alloys and Compounds 509 (2011) 4992–4998

Contents lists available at ScienceDirect

Journal of Alloys and Compounds

journal homepage: www.elsevier.com/locate/jallcom

Flow stress modeling of AZ91 magnesium alloys at elevated temperature

B.K. Raghunath[a], K. Raghukandan[a], R. Karthikeyan[b], K. Palanikumar[c,*], U.T.S. Pillai[d], R. Ashok Gandhi[e]

[a] Department of Manufacturing Engineering, Annamalai University, Chidambaram, India
[b] Department of Mechanical Engineering, BITS-Pilani, Dubai Campus, United Arab Emirates
[c] Department of Mechanical Engineering, Sri Sai Ram Institute of Technology, Sai Leo Nagar, Chennai 600 044, India
[d] Regional Research Laboratory, Trivandrum, India
[e] Department of Mechanical Engineering, Sri Sai Ram Engineering College, Sai Leo Nagar, Chennai 600044, India

ARTICLE INFO

Article history:
Received 3 August 2010
Received in revised form 26 January 2011
Accepted 27 January 2011
Available online 26 February 2011

Keywords:
Flow stress
Magnesium alloy
Zener–Hollomon parameter

ABSTRACT

The flow curve is constructed by flow stress data obtained from compression test conducted at different temperature and strain rate. Accurate flow stress model is crucial for investigating magnesium alloys deformation behaviour at the elevated temperatures. An analytical method, which reflects temperature, strain and strain rate effect by introducing temperature-compensated strain rate (Zener–Hollomon Parameter), is proposed in this study. This model has been applied on the experimental data and predicted flow stress curve match well with those measurements.

1. Introduction

In a world becoming more and more conscious of environment and safety, automobile manufacturing industries are obliged to produce lighter vehicles, with lower density of 1.74 g/cnv, high specific strengths and electromagnetic interference shielding capacities, magnesium alloys are being manufactured increasingly for light weight structural and functional parts in the automotive and electronic industries [1,2]. Presently, magnesium alloys are mainly processed by die casting or thixo-forming processes [3]. However, the die casting magnesium products have disadvantages, such as pin holes, porosity, cold shuts and low strength. Although semisolid methods, such as thixomolding or rheomolding, can reduce the scraping rate of castings, the high temperature caused die erosion and part problems still need to be solved for industrial practice. Forming processes is a promising solution for the problem by offering fine-grained microstructure without porosity [4]. Due to the fact that closed-packed hexagonal (CPH) lattice structure magnesium alloys have limited ductility at the room temperature, the forming processes need to be conducted at elevated temperatures from 200° to 400 °C, which activates additional pyramidal slip systems in the hexagonal structure [1]. As a powerful tool to study the forming process, FEM simulation is used increasingly and a proper flow stress description is the preliminary requirement for an accurate prediction [5]. Many models have been proposed to describe the flow stress and an extensive summary on different flow stress models is given in [6]. Based on an observation of a linear relationship between semi-log Zener–Holloman parameter and proof stress, Takuda et al. [7] proposed a parametrical method to express the proof stress of magnesium-based alloys AZ31 and AZ91 in hot working processes. They derived a formula by analyzing the stress data measured at various temperatures and strain rates. The formula is expressed in a simple form by means of the temperature-compensated strain rate, i.e., the Zener–Hollomon parameter. Similar method is applied successfully on hot extrusion tests on Mg–8A1 alloys by Yang and Koo [8]. The authors Takuda et al. [7] and Yang and Koo [8] have used the tensile test data for hot extrusion of magnesium based AZ31 and AZ91 alloys and Mg–8A1 alloys respectively. The method proposed by these authors does not consider the strain effect on flow stress, which is critical for the accurate prediction of metal deforming process. In the present study compression test results are used for constructing flow stress curve. An analytical method is proposed for constructing the model. The results indicated that the predicted flow stress curve match well with the experimental results.

2. Flow stress prediction

In this study, a Zener–Hollomon parameter based analytical method is introduced and demonstrated for AZ91 Mg alloy. Since Zener–Hollomon parameter works at a narrow temperature and

* Corresponding author. Tel.: +91 44 22512333; fax: +91 44 22512323.
E-mail addresses: bkrau@rediffmail.com (B.K. Raghunath), palanikumar_k@yahoo.com (K. Palanikumar), ashokgandhir@yahoo.co.in (R.A. Gandhi).

0925-8388/$ – see front matter © 2011 Elsevier B.V. All rights reserved.
doi:10.1016/j.jallcom.2011.01.182

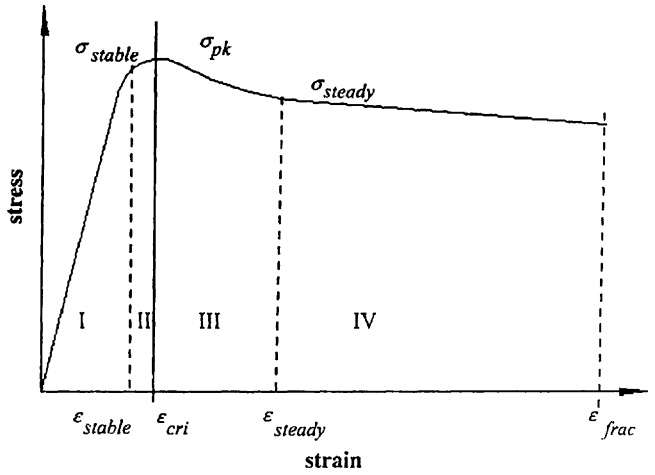

Fig. 1. Typical flow stress curve at the elevated temperature.

strain rate ranges, the investigated experimental data are within a temperature range from 300 to 500 °C and a strain rate range from 0.001 to 1 s^{-1}. Zener–Holloman parameter value for AZ91 Mg alloy is calculated by Eq. (1). Based on the above analysis, it is observed that the flow stress is composed of different stages and strongly affected by the Zener–Hollomon parameter. At an assumption that the designed experiments reflect the trend of temperature and strain rate effect on the flow stress, a Zener–Hollomon parameter model is proposed.

The authors have interpolating the results by considering different stages rather than a direct parametric interpolation for experimental results over the whole strain–stress curve. Even-though the polynomial interpolation or a spline based interpolation with coefficient depending on the Zener–Hollomon parameter Z is simple, the authors have adopted this method because in this method beginning flow stress and strain value of each stage is calculated, further the effect of Zener–Hollomon parameter on the critical strain for softening, beginning strain for steady stage is inferred, which can be useful for micro level analysis.

2.1. Deformation mechanism of Mg alloys at the elevated temperature

At elevated temperatures, a typical flow stress which is composed of four stages, as illustrated in Fig. 1, is a combined effect of work hardening, which is primarily caused by second-order pyramidal slip system (c + a) dislocation motion and thermally activated softening [9].

Work hardening stage I: hardening rate is higher than the softening rate and thus the stress rises steeply at micro strain deformation (0.1–1%) then increases at a decreased rate.

Stable stage II: an equilibrium between the dislocation generation and annihilation rate is obtained thus a short stable stage exhibits. The stable stage will be ended by next stage.

Softening stage III: in which the dislocations are annihilated in large numbers through the migration of a high angle boundary and the stress drops steeply.

Steady stage IV: the stress becomes steady when a new balance between softening and hardening is obtained.

Flow stress is affected by many factors, such as alloying composition [10], microstructure [11,12], texture and deformation mode, temperature and deformation speed [13]. At given material properties, the shape of flow curve is primarily affected by deformation mode, strain rate and temperature.

2.2. Deformation mode

As a polycrystalline metal with CHP structure, the deformation of magnesium alloys is caused by the resolved shear stress sliding atoms while the norm stress pulling or compressing the atoms apart or close [9]. According to Takuda et al. [11], at the strain rate range (0.001–1 s^{-1}) the compression dominant tests can increase the fracture/crack strain (ε_{frac}), from a range of 0.1–0.37 in tensile tests to a range from 0.6 to 1.4 in compression tests [14].

Deformation mode also affects the shape of flow stress curves. In the compression test, stress playing dominant role in the extrusion and upsetting. A stress–strain curve sequentially exhibits work hardening stage, stable stage, softening stage and steady stage. In tensile test, when the temperature is lower and/or strain rate is higher, stress–strain curves only exhibit work hardening stage and/or stable stage while at the higher temperature and lower strain rate, the curves exhibit both work hardening, stable and softening stages. In the pure shear stress status, the stress–strain curves stay in the work hardening regime in a strain up to 0.5.

2.3. Deformation speed and temperature effect

The effect of deformation speed and temperature on flow stress traces can be explained by the terms of dynamic recrystallization and dislocation mechanism in polycrystalline metals. Dynamic recrystallization phenomenon is sensitive to the temperature and processing time. Lower strain rates and higher temperatures provide longer time for energy accumulation and higher mobility at boundaries for the nucleation and growth of dynamically recrystallized grains and dislocation annihilation and thus reduce the flow stress level. On the contrary, lower temperature and higher strain rate increases the flow stress.

The combined effect of temperature and deformation speed can be expressed by the Zener–Hollomon parameter (temperature-compensated strain rate) as following [15]:

$$Z = \dot{\varepsilon} \exp\left(\frac{Q}{RT}\right) \tag{1}$$

where $\dot{\varepsilon}$ is the strain rate (s^{-1}), R is the universal gas constant (8.314 J mol^{-1} K^{-1}), T is the absolute temperature, Q is the activation energy for the deformation, for the consistency, it is chosen as 135 kJ/mol for Mg alloy. Activation energy (Q) can be calculated from flow stress data using sine relationship [16].

$$Q = K_1 \frac{R}{m} = K_1\, R n_1 \quad (\text{kJ/mol}), \quad \text{where} \quad n_1 = \frac{1}{m} \tag{2}$$

The temperature sensitivity (K_1) and strain rate sensitivity (m) for AZ91 Mg alloy is obtained by the plot between log stress vs. absolute temperature (Fig. 2) and log stress vs. log strain rate (Fig. 3) respectively, from the data given in Table 1.

Activation energy at various strains is depicted in Fig. 4. Activation energy keeps on decreasing from 157 kJ/mol at different strain. The value of activation energy is in the range of 150–157 kJ/mol, which is closer to self diffusion of AZ91 Mg alloy (134 kJ/mol).

2.4. Hardening and stable stage

At the hardening stage of the flow curve, the stress increases rapidly at the micro strain range (<0.2%: yield stress or proof stress) then increase rate drops gradually until a stable state is obtained. Since the time and temperature are two factors determining the accumulated energy to activate and facilitate the movement of slip systems, the stress level and slope of the flow stress curve are sensitive to temperature and strain rate. Takuda et al. [17] observed the proof stress level increases linearly with the semi-log scaled Zener–Hollomon parameter value in uniaxial tension

Table 1
Flow stress data for AZ91 Mg alloy at different temperatures, strain rates and strains.

Strain rate (s^{-1})	Strain	Flow stress (MPa)				
		300 °C	350 °C	400 °C	450 °C	500 °C
0.001	0.1	60	39	30	21	9.5
	0.2	53	40.5	28.7	20.6	9.15
	0.3	52.8	38.7	27.5	20.12	8.9
	0.4	51.5	35.5	26.3	19.9	8.85
	0.5	50.9	35.25	26.12	20.5	8.26

Table 2
K value for AZ91 Mg alloy for different strain rates.

Temperature (°C)	Strain	Strength component *K* (in MPa)			
		0.001 s^{-1}	0.01 s^{-1}	0.1 s^{-1}	1 s^{-1}
300	0.1	57.75	80.81	110.20	131.29
	0.2	54.26	78.60	107.12	126.76
	0.3	52.31	77.30	105.14	124.10
	0.4	50.98	76.40	103.76	122.34
	0.5	49.96	75.71	102.43	120.94

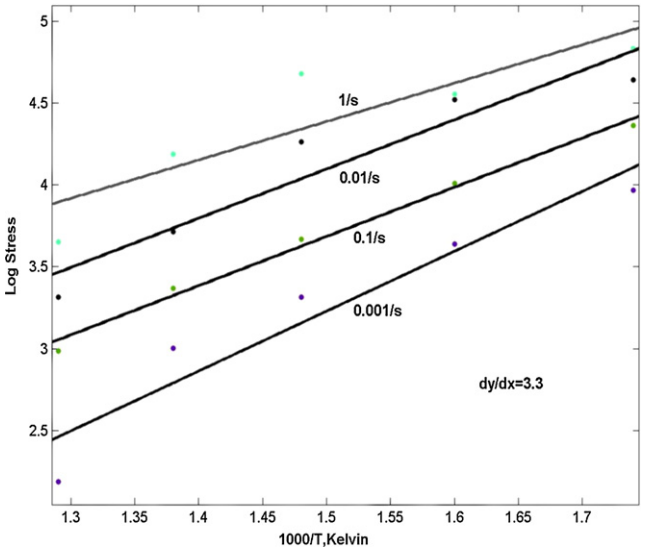

Fig. 2. Determination of strain rate sensitivity (m) and temperature sensitivity (K_1) for AZ91 Mg Alloy at 0.3 strain.

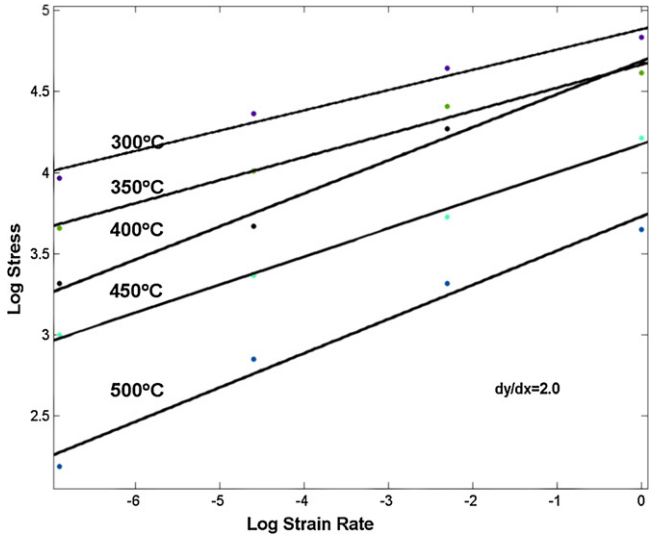

Fig. 3. Determination of strain rate sensitivity (m) and temperature sensitivity (K_1) for AZ91 Mg Alloy at 0.3 strain.

tests on Mg–Al–Zn alloys and Mg–8A1 sheet, respectively. Hollomon equation $\sigma = k\varepsilon^n$ [18], in which K the strength component and n the work-hardening exponent represent stress level and work hardening tendency, are chosen to describe flow stress curve. The temperature and strain rate effect on work hardening and stress level is described by Zener–Holloman parameter effect on n and K at semi-log scale. K values for AZ91 Mg alloy is determined at different strain rates and temperatures are given in Tables 2 and 3.

Fig. 5 is plotted between Z parameter and strength coefficient (K). It shows that strength coefficient increases linearly as Z value increases, suggesting that strength component of the Mg alloy increases with increase in temperature and strain rate. Similar trend is observed in Fig. 6, work hardening index (n) increases with increase in temperature and strain rate.

Hence, the work hardening index n and strength coefficient K are strongly influenced by Zener–Hollomon parameter. Thus, equation $\sigma = K\varepsilon^n$ is extended to express both temperature and strain rate effect as following equation:

$$\sigma = K(Z)\varepsilon^{n(Z)}, \quad \varepsilon_{0.002} < \varepsilon \leq \varepsilon_{\text{stable}} \tag{3}$$

Table 3
K value for AZ91 Mg alloy for different temperatures.

Strain rate s^{-1}	Strain	Strength component *K* (in MPa)				
		300 °C	350 °C	400 °C	450 °C	500 °C
0.001	0.1	57.75	40.21	30.02	21.28	9.25
	0.2	54.26	38.3	28.29	20.36	9.16
	0.3	52.31	37.23	27.28	19.29	8.85
	0.4	50.98	36.49	26.58	18.69	8.50
	0.5	49.96	35.92	26.05	18.05	8.10

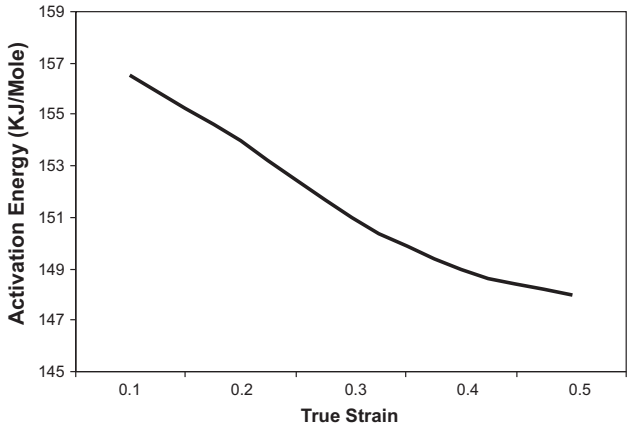

Fig. 4. Activation energy at different strain for AZ91 Mg alloy at 300 °C.

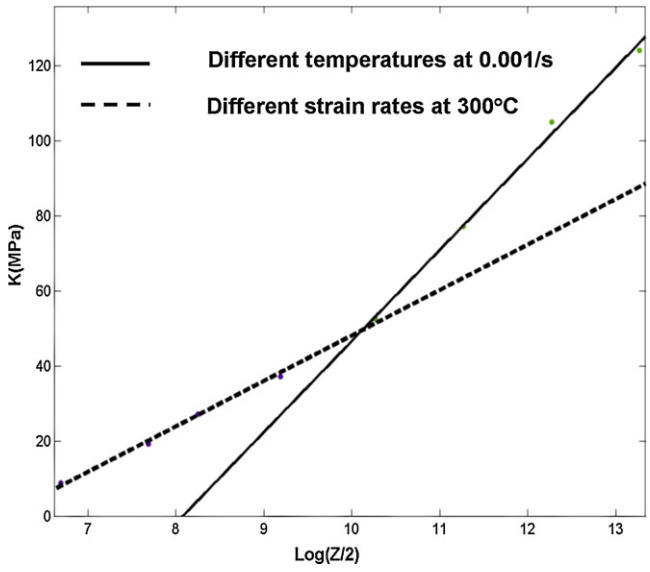

Fig. 5. Z parameter vs. strength coefficient for AZ91 Mg alloy.

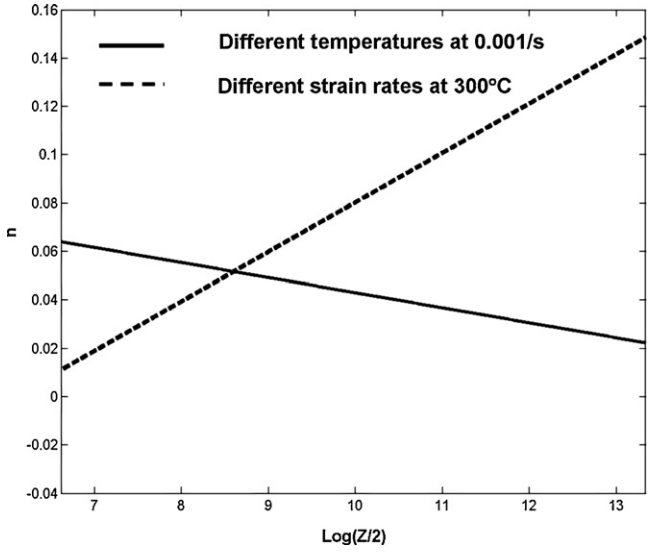

Fig. 6. *Z* parameter vs. work hardening index, *n*.

Table 4
Constants for AZ91Mg alloy at various stages.

Constants	Value
A_1	0.4431 MPa
B_1	−0.0426 MPa
C_1	5.45 MPa
A_2	0.0021
B_2	−0.1034
C_2	0.9021
E	−17.358 MPa
F	154.58 MPa
H	−0.858 MPa
I	8.214 MPa
L_{stable}	0.0052
M_{stable}	0.0036
L_{sft}	0.016
M_{sft}	−0.0543
L_{steady}	0.0312
M_{steady}	−0.1451
α	20 MPa

while the $K(Z)$ and $n(Z)$ are represented by two order polynomial equations:

$$K(Z) = A_1\left(\log\left(\frac{Z}{2}\right)\right)^2 + B_1\ \log\left(\frac{Z}{2}\right) + C_1 \quad (4)$$

$$n(Z) = A_2\left(\log\left(\frac{Z}{2}\right)\right)^2 + B_2\ \log\left(\frac{Z}{2}\right) + C_2 \quad (5)$$

The constants A_1, A_2, B_1, B_2, C_1 and C_2 can be determined by regression on the experimental data and are given in Table 4. Based on the identification of a linear relationship between semi-log scaled Z and flow stress in [10], $Z/2$ is used in this study. Stable stress can be predicted by calculating $K(Z)$ and $n(Z)$ by using Eqs. (4) and (5) and applying these values in Eq. (3).

At the stable stage, flow stress does not vary obvious and a linear equation is applied to express the evolution as following:

$$\sigma = \sigma_{stable} + \alpha(\varepsilon - \varepsilon_{stable}), \quad \varepsilon_{stable} < \varepsilon \le \varepsilon_{cri} \quad (6)$$

where σ_{stable} is the stress value at the end of hardening stage and α is the slope of stable stage and can be determined by regression on the experimental data.

Temperature and strain rate also affect the length of hardening stage, which is represented by the beginning of stable stage. The relationship between Zener–Hollomon value and normalized stable stage strain ($\varepsilon_{stable}/\varepsilon_{frac}$) from flow curve is illustrated in Fig. 7 which shows the value of $\varepsilon_{stable}/\varepsilon_{frac}$ increases with the Zener–Hollomon value. Same trend is also found between Zener–Hollomon parameter and normalized critical strain for softening $\varepsilon_{cri}/\varepsilon_{frac}$ (Fig. 8), which confirms, the observation in [13]. The physical explanation of this phenomenon is that high temperature and lower strain rate can accumulate enough energy for recrystallization at a shorter deformation range, on the contrary, lower temperature and higher strain rate delays the happening of stable and softening stage.

2.5. Softening and steady stage

The presence of a distinct peak in the flow stress (Fig. 1) indicates the beginning of recrystallization softening. The dynamic recrystallization process depends on time and temperature, higher strain rate and lower temperature lead to a higher peak stress and thus need larger deformation (strain) for nucleation and growth of dynamically recrystallized grains. The slope of softening stage is also affected by Zener–Hollomon parameter (Z) and a linear equation is given to describe the flow stress at this stage:

$$\sigma_{sf} = \sigma_{pk} + D(Z)\ \ (\varepsilon - \varepsilon_{cri}), \quad \varepsilon_{cri} < \varepsilon \le \varepsilon_{steady} \quad (7)$$

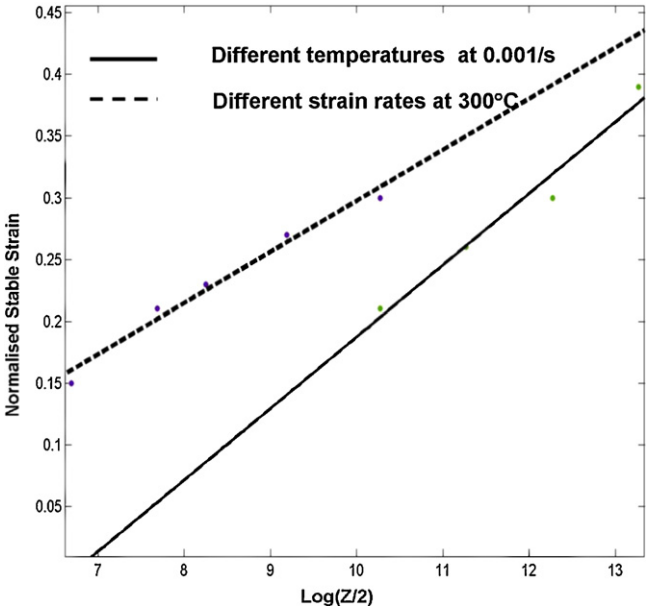

Fig. 7. Z parameter vs. normalized stable strain.

where σ_{pk} is the peak stress, ε_{cri} is the corresponding critical strain, as seen in Fig. 1.

$D(Z)$ is the slope of the softening stage and can be described by:

$$D(Z) = E\,log\left(\frac{Z}{2}\right) + F \tag{8}$$

Similar linear equation is also applied on the steady stage as following:

$$\sigma = \sigma_{sft} + G(Z)\ \ (\varepsilon - \varepsilon_{steady}), \quad \varepsilon_{steady} < \varepsilon \leq \varepsilon_f \tag{9}$$

where σ_{sft} is the stress at the end of softening stage and ε_{steady} is the strain for the steady stage beginning, as seen in Fig. 1.

$G(Z)$ is the slope of the steady stage and can be described by:

$$G(Z) = H\,log\left(\frac{Z}{2}\right) + I \tag{10}$$

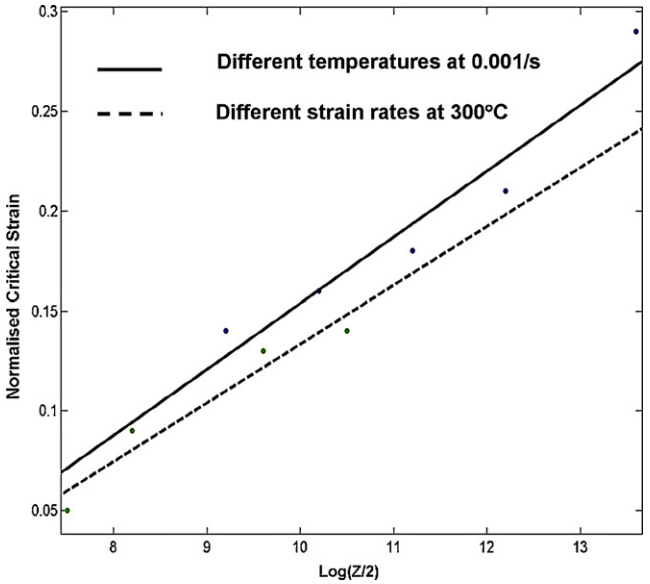

Fig. 8. Z parameter vs. normalized critical strain.

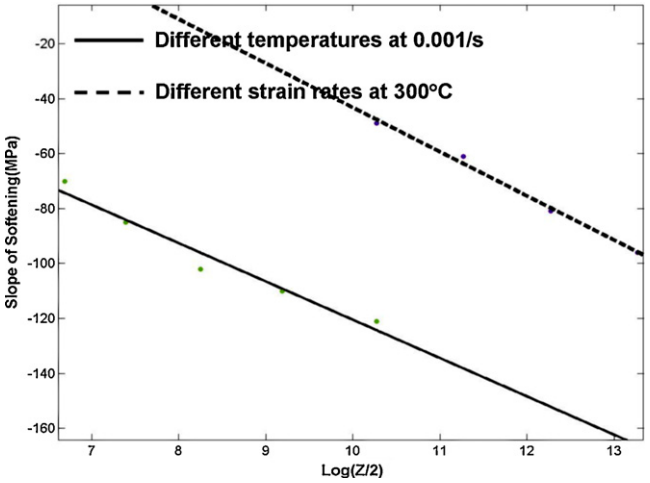

Fig. 9. Z parameter vs. slope of softening stage.

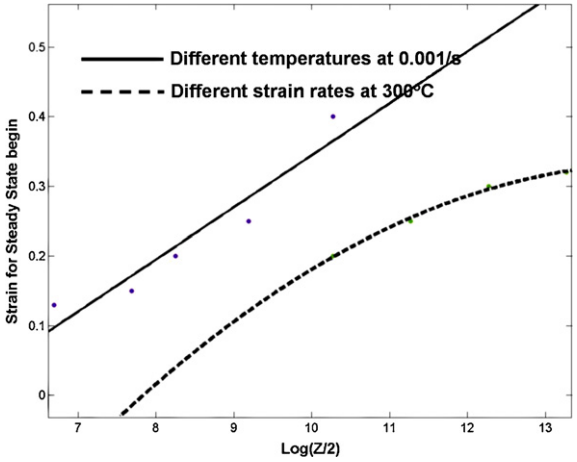

Fig. 10. Z parameter vs. strain for steady state begin.

Constants E, F, H, I in above equations can be determined by linear regression on the experimental data.

The effect of Zener–Hollomon parameter on the critical strain for softening, beginning strain for steady stage, slope of softening stage and steady stage for AZ91Mg alloy is illustrated in Figs. 9–11. It is

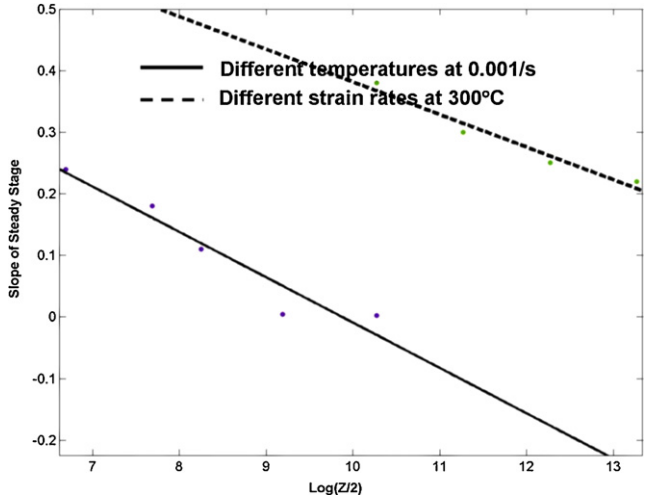

Fig. 11. Z parameter vs. slope of steady stage.

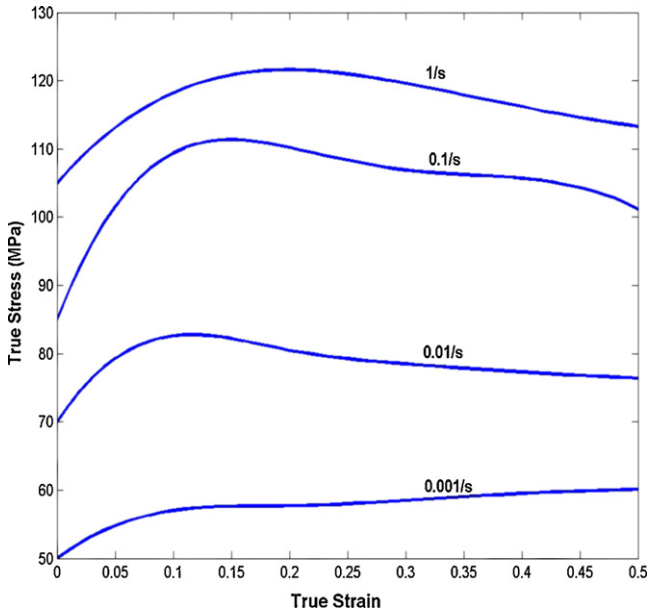

Fig. 12. Flow curve for AZ91 Mg alloy at 0.001 s^{-1} with different temperature and at 300 °C with different strain rate.

found that higher Zener–Hollomon value delays the beginning of softening and steady state stages and corresponding steeper slope values.

2.6. Transfer of different stages

For the reason explained in various stages, the beginning strains of different stages are determined by the Zener–Hollmon parameter (Z) and formulated into a linear equation as follows:

$$\varepsilon_i(Z) = L_i \ log\left(\frac{Z}{2}\right) + M_i, \quad i \in \{\text{stable}, \quad \text{cri}, \quad \text{steady}, \quad \text{frac}\} \qquad (11)$$

where constant L_i and M_i can be determined by the linear regression on the experimental data. The constants at various stages as mentioned above are calculated by using Eqs. (3)–(11) and are listed in Table 4.

The Zener–Holloman parametrical method is applied to the flow curves shown in (Figs. 12 and 13). Predicted flow stress at various stages of flow curve (300 °C and at 0.001 s^{-1}), at predicted strain are calculated as shown below. Predicted strain at various stages is calculated by Eq. (11).1. At hardening stage, $K(Z) = 58.27$, $n(Z) = 0.04$, stable strain is 0.08,

$$\sigma_{\text{stable}} = 57.66$$

2. At softening stage, $\sigma_{\text{pk}} = 61$, $D(Z) = -44.90$ from Eq. (9), softening strain is 0.2

$$\sigma_{\text{sft}} = 52.02$$

3. At steady stage, $\sigma_{\text{sft}} = 52.02$ $G(Z) = 0.492$ from Eq. (11) steady strain is 0.35

$$\sigma_{\text{steady}} = 52.19$$

Similarly the same procedure is adopted for the remaining flow curves as in Figs. 12 and 13, at different stages for predicted flow stress.

In this work, the processing map for AZ91 Mg alloy have been developed and the DRX domain is lies in the range of 340–440 °C and at a strain rate in the range of 0.01–0.1 s^{-1}. The flow instability has occurred, at higher strain rates and the temperature above

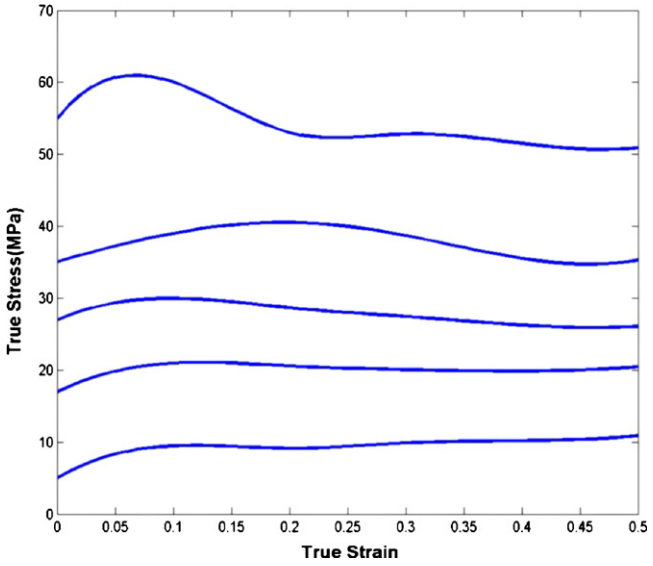

Fig. 13. Flow curve for AZ91 Mg alloy at 0.001 s^{-1} with different temperature and at 300 °C with different strain rate.

500 °C. This corresponds to adiabatic shear band and matrix cracking. Forming this material above 500 °C is not advisable; hence the domain of temperature and strain rates are constrained.

The comparison between measured flow stress and predicted flow stress is plotted in Figs. 14 and 15. Comparisons show that the flows stress predicted by the proposed method match well with that measured from experiments.

3. Prediction and verification

The proposed method has been applied on the experimental test shown in Figs. 12 and 13. The calculated constant for the prediction model are listed in the Table 4, which are corresponding to experimental data. Comparisons on the calculated flow stress curves and measured results are given in Figs. 14 and 15. It is found that the maximum difference between the calculated curves and the measured ones is lower than 8%.

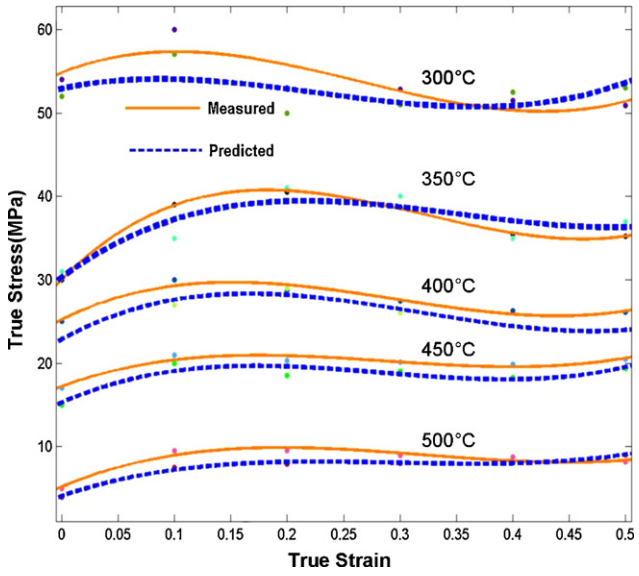

Fig. 14. Comparison of predicted flow stress with measured results for AZ91 Mg alloy at 0.001 s^{-1} and at 300 °C.

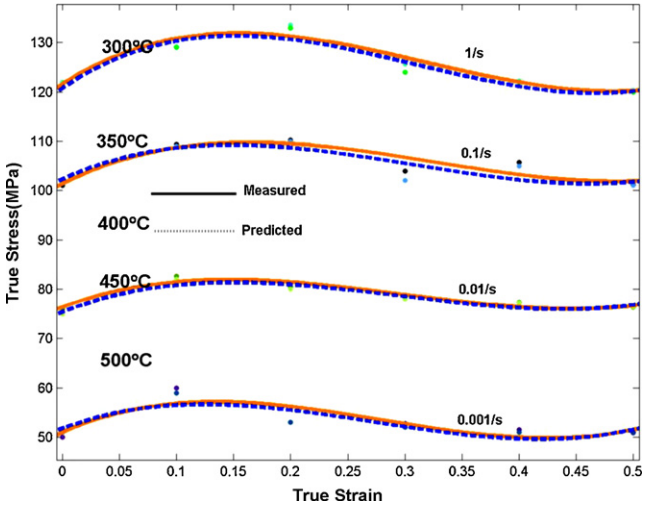

Fig. 15. Comparison of predicted flow stress with measured results for AZ91 Mg alloy at 0.001 s^{-1} and at 300 °C.

4. Conclusions

Based on the analysis on magnesium alloy deformation mechanism at elevated temperatures and different strain rate, an analytical model is proposed to describe the flow stress evolution in this study. Zener–Holloman parameter is introduced to reflect the combination effect of temperature and strain rate. The model has been verified on three published experimental results. Comparisons show that the flow stresses predicted by the proposed model match well with that measured from experiment.

Acknowledgement

Our heartiest thanks to Dr. U.T.S. Pillai, Scientist, Regional Research Laboratory, Trivandrum, India., for supplying the casting material for carrying out this investigation.

References

[1] B.L. Mordike, T. Ebert, Mater. Sci. Eng. A 302 (2001) 37–45.
[2] T. Sana, T. Saiki, S. Horikoshi, S. Fuchizawa, S. Sado, Proceedings of the International Workshop Environmental and Economic Issues Metal Processing, Nara, Japan, 1998, pp. 57–63.
[3] H.E. Boyer, T.L. Gall, Metals Handbook, 44073, second ed., ASM, Metals Park, Ohio, 1985.
[4] E. Doege, K. Drbder, J. Mater. Process. Technol. 115 (2001) 14–19.
[5] A. Gavrus, E. Massoni, J.L. Chenot, J. Mater. Process. Technol. 60 (1996) 447–454.
[6] Z. Gronostajski, J. Mater. Process. Technol. 106 (2000) 40–44.
[7] H. Takuda, H. Fujimoto, N. Hatta, J. Mater. Process. Technol. 80–81 (1998) 513–516.
[8] W.G. Yang, C.H. Koo, Bulletin of the College of Engineering, N.T.U., No. 89, October, 2003, pp. 63–82.
[9] R.E. Smallman, R.J. Bishop, Modern Physical Metallurgy and Materials Engineering, Sixth ed., Burterworth-Heinemann, 2002.
[10] M.R. Barnett, Acta Mater. 55 (9) (2007) 3271–3278.
[11] H. Takuda, H. Fujimoto, N. Hatta, Mater. Process. Technol. 80–81 (3) (1994) 349–360.
[12] J. Kusiak, R. Kawalla, M. Pietrzyk, H. Pircher, Mater. Process. Technol. 60 (1–4) (1996) 455–461.
[13] C. Zener, J.H. Hollomon, Appl. Phys. 15 (1944) 22–32.
[14] E. Doege, K. Dröder, Mater. Process. Technol. 115 (1) (2001) 14–19.
[15] R. Shivpuri, Z.Q. Sheng, Mater. Sci. Eng. A 419 (2006) 202–208.
[16] H.J. Forst, M.F. Ashby, Deformation Mechanism Maps, Pergamon, Oxford, 1982, pp. 44–50.
[17] H. Takuda, S. Kikuchi, T. Tsukada, K. Kubota, N. Hatta, Mater. Sci. Eng. A 271 (1–2) (1999) 251–256.
[18] Z. Gronostajski, Mater. Process. Technol. 157–158 (2004) 165–170.